

Dark sector spectroscopy at the ILC

Jeppe R. Andersen^{1,a}, Michael Rauch^{2,b}, Michael Spannowsky^{1,c}

¹ Department of Physics, Institute for Particle Physics Phenomenology, Durham University, Durham, UK

² Institute for Theoretical Physics, Karlsruhe Institute of Technology (KIT), Karlsruhe, Germany

Received: 17 February 2014 / Accepted: 15 May 2014 / Published online: 7 June 2014

© The Author(s) 2014. This article is published with open access at Springerlink.com

Abstract Recent studies have shown that searches in the mono-photon and missing energy final state can be used to discover dark matter candidates at the ILC. While an excess in this final state over the Standard Model background would indicate the existence of a dark sector, no detailed information about the internal structure of this sector can be inferred. Here, we demonstrate how just a few observables can discriminate between various realisations of dark sectors, including e.g. the spin of mediators.

1 Introduction

Astronomical observations strongly indicate the existence of dark matter [1–5]. Many extensions of the Standard Model take this into account by incorporating a so-called dark sector: a sector of particles that do not carry electric or color charge. The interactions of the dark sector can be protected by global symmetries and the particles can have a long lifetime. Often the dark sector is not completely decoupled, but it interacts with the Standard Model particles by the exchange of a Z boson, or a mediator of a yet unknown force.

In recent years several experiments, i.e. PAMELA [6, 7], Fermi LAT [8] and most recently AMS [9], have observed an excess in the positron fraction in the electron–positron energy spectrum at energies above ~ 10 GeV. A possible explanation for this excess could be the decay of an invisible particle into an e^+e^- pair. Leptophilic dark sectors have been identified as a possible explanation of the observed excess [10–15].

Unfortunately, due to the large uncertainties in evaluating the astrophysical backgrounds, indirect detection experiments face challenges in claiming the discovery of a potential dark matter candidate. Direct detection experiments try to measure the momentum transfer between the weakly inter-

acting massive particle (WIMP) and the detector. If the WIMP is light, the sensitivity of the experiments is strongly reduced [16, 17]. Interpretations of searches for WIMPs at direct detection experiments usually assume that the dark sector is minimal, i.e. consists of only one particle, and the WIMP accounts for the total dark matter abundance in the universe. We will not make those strong assumptions. Indeed, if the dark sector is not minimal, constraints from direct detection experiments are strongly relaxed.

Another possibility to evade the bounds from detection experiments is that the dark sector particle (DSP) is not even stable on cosmological time scales, and might even be unconnected to the dark matter solution. For high-energy collider experiments, it is sufficient that the DSP has a life time of the order of microseconds to give a signature of missing transverse momentum only, or even that it does not decay back into detectable Standard Model particles with a large enough rate.

Recently it has been pointed out that in case the DSP couples with reasonable strength to quarks, mono-jet searches at the Tevatron and LHC can be a superior way in discovering them [18–26]. If the DSP couples predominantly to leptons, constraints can be derived from LEP in mono-photon searches [27] or a future electron–positron collider [28].

Unfortunately, both direct detection experiments and mono-jet/mono-photon searches are very limited tools in unravelling the detailed structure of the dark sector, e.g. the spin of the force mediator in combination with its mass and the mass of the DSP(s). In mono-photon searches the DSPs recoil against a high-pT photon. Therefore, only the total amount of missing transverse energy in the event can be measured, i.e. the differential cross section for one observable.

The observables discussed in this article allow an unbiased view into the dark sector, as long as a mediator couples the dark sector to electrons. Because of the lack of an existing electron–positron collider we will discuss these observables in the context of the International Linear Collider (ILC, 500 GeV beam energy). So far, the ILC's great potential in

^a e-mail: jeppe.andersen@durham.ac.uk

^b e-mail: michael.rauch@kit.edu

^c e-mail: michael.spannowsky@durham.ac.uk

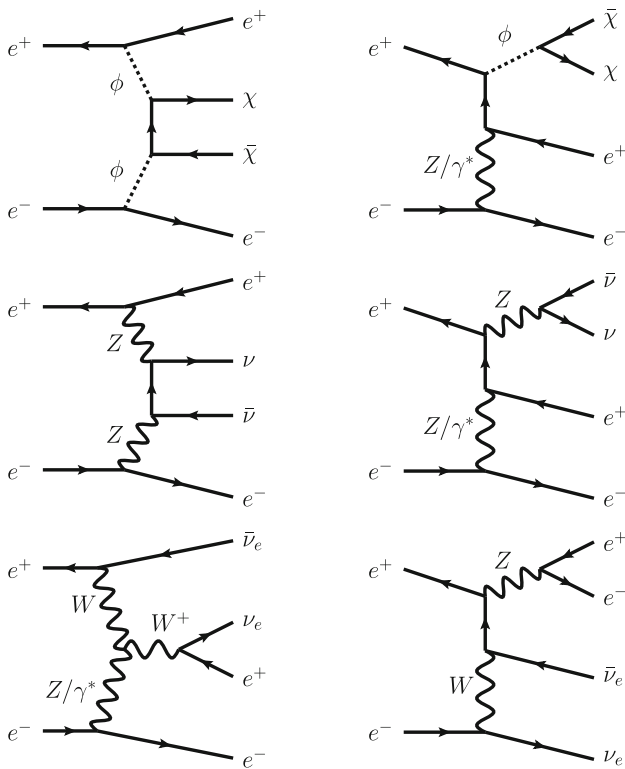


Fig. 1 Representative Feynman diagrams for the process considered in this article. The *top row* shows the signal process with mediator ϕ and DSP χ , while the *middle and bottom row* depict Standard Model backgrounds, where ν without index denotes a neutrino of any generation

studying the structure of dark sectors has not been completely appreciated [29, 30]. We assume that the particles in the dark sector are stable on collider time scales and escape detection at the LHC. Therefore, our signal will consist of electrons and missing energy, i.e. our process is $e^+e^- \rightarrow e^+e^- + E_{T,miss}$. This signature is relatively rare in the Standard Model, predominantly generated in the production of Z bosons and photons with subsequent decay/splitting to an e^+e^- pair and neutrinos. Some example Feynman diagrams for both signal and background processes are depicted in Fig. 1.

An important topology for the study of the structure of the dark sector is the so-called vector boson fusion (VBF) topology (i.e., two possibly forward well-separated electrons), even though the DSPs are not necessarily produced by exchanging a vector boson. Tight cuts on the electron-positron system can reduce the Standard Model backgrounds and increase the average energy flowing through the DSP- e^+e^- coupling. A similar strategy is used when studying the coupling structure of the Higgs boson to quarks: Producing a Higgs boson in the VBF channel, angular correlations of the jets can be used to distinguish a CP-even from a CP-odd Higgs boson [31–33] and an invisibly decaying Higgs boson can be disentangled from the backgrounds [34]. Similar kine-

matic configurations can be used to study dark sectors with DSP-quark couplings at the LHC. However, we find that at the LHC the DSP-quark coupling has to be of the order of the electroweak coupling to give a significant event shape contribution, reflected in the invariant mass $m_{jj} = \sqrt{(p_{j1} + p_{j2})^2}$ or the rapidity difference $\Delta y_{jj} = |y_{j1} - y_{j2}|$ of the two so-called tagging jets, the two jets with the largest transverse momentum. Furthermore, at the LHC large systematic uncertainties in final states with missing transverse energy (MET) and jets render a dark sector spectroscopy a difficult task [35].

This article is organised as follows: In Sect. 2 we discuss our benchmark models and assumptions which specify the DSPs–electron–positron interactions. Kinematic observables are identified and interpreted in the context of Regge theory in Sect. 3. We further evaluate how well the different benchmark models can be discriminated. In Sect. 4 we present our conclusions.

2 Benchmark models and experimental constraints

For simplicity we assume that the DSP is a Dirac fermion. We have also investigated scenarios where the DSP is a scalar instead, but we find no significant differences compared to the Dirac case. As we will see later in Sect. 3, such a behaviour is expected, as we are predominantly sensitive to the mass of the DSP only. The mediator can be either a scalar particle or a vector particle, which couples only electrons from the Standard Model to the dark sector. Extending this coupling to all SM leptons would be straightforward. The only place where this matters is the width of the mediator particle, which gets increased by additional couplings to muons and taus. The width is calculated using the program BRIDGE [36]. As the width turns out to be small for the coupling values considered in the following, taking for example a generation-blind scenario instead would have no relevant effect on our results. We also assume that the coupling between mediator and neutrino vanishes. If such a coupling was of the same strength as those to electrons, this would yield an additional contribution to the mono-photon searches, as it has the same signature, and is therefore significantly constrained.

The interaction terms appearing in the Lagrangian are denoted in Table 1.

Table 1 Terms in the Lagrangian describing interactions between the mediator and the electron or the DSP particle

	Scalar	Vector
e	$g_{ee\phi,S} \bar{e}e\phi_S$	$g_{ee\phi,V} \bar{e}\gamma_\mu e \phi_V^\mu$
χ	$g_{\chi\chi\phi,S} \bar{\chi}\chi\phi_S$	$g_{\chi\chi\phi,V} \bar{\chi}\gamma_\mu\chi\phi_V^\mu$

Table 2 Overview of the different model scenarios used in our analysis. The first and third letter of the model name denote the mass (light or heavy) of the mediator and DSP, respectively, while the middle one describes the spin nature of the mediator (scalar or vector)

Model	Mediator mass (GeV)	Mediator spin	DSP mass (GeV)	M_* (GeV)
LSL	8	0 (scalar)	5	30
LVL	8	1 (vector)	5	30
LSH	8	0 (scalar)	120	27.4
LVH	8	1 (vector)	120	21
HSL	200	0 (scalar)	5	1250
HVL	200	1 (vector)	5	1250
HSH	200	0 (scalar)	120	332.4
HVH	200	1 (vector)	120	511.8

Our analysis uses light mediator particles. Therefore, the momentum dependence in the propagator of the mediator plays an important role and cannot be neglected. Hence, it is not possible to formulate the results in terms of an effective dimension-six operator of the form $\bar{e}e\bar{\chi}\chi$ or $\bar{e}\gamma_{\mu}e\bar{\chi}\gamma^{\mu}\chi$ for scalar or vector mediator, respectively, where the mediator is integrated out. Nevertheless, one can still define an effective mass M_* as

$$M_* = \frac{M_{\phi}}{\sqrt{g_{ee\phi}g_{\chi\chi\phi}}} \tag{1}$$

as in Reference [25]. In the limit of a heavy mediator, the term $1/M_*^2$ becomes the prefactor of the dimension-six operator.

In the following, we define eight different model scenarios. They are characterised by three different options, namely the spin and mass of the mediator particle and the mass of the DSP. For the spin of the mediator particle we investigate the two possibilities already mentioned, namely a scalar and a vector particle. In many scenarios the dark sector is linked to the Standard Model via kinetic mixing of a dark photon of a hidden $U(1)$ with the $U(1)$ hypercharge of the Standard-Model [37–40]. In the scalar case we assume that the mediator couples chirally and exclusively to electrons and DSPs. By measuring the spin of the mediator such models can be either confirmed or disfavoured.

For the two masses we define a light and a heavy scenario each, with values of 8 and 200 GeV for the mediator particle and 5 and 120 GeV for the DSP mass.

An overview is shown in Table 2 together with the effective mass M_* used for each scenario. The exact choice of masses is somewhat arbitrary, but it has been guided by the following considerations. The mass of the light DSP is chosen such that it is below the typical reach of direct detection experiments, while the heavy scenario has a mass which is beyond the reach of direct searches at LEP. The two choices for the mediator mass have then been chosen such that in the light–light and

heavy–heavy models the on-shell decay of a mediator particle into two DSPs is kinematically forbidden.

The coupling parameters for the light DSP models are already constrained by direct searches at LEP. Therefore, we choose our effective mass such that they are at the 90 % CL exclusion boundary given in Reference [25]. For the 200 GeV mediator the effective mass parameter can be taken directly from there, while for the 8 GeV mediator we have instead used the given value for the 10 GeV curve. This is slightly more restrictive than the true 8 GeV value, so with this choice we are erring on the safe side. The heavy DSP scenarios with a DSP mass of 120 GeV are beyond the reach of LEP. As the mediator couples only to electrons, also searches at hadron colliders cannot significantly constrain the coupling parameters. Only a direct interpretation of the DSP as dark matter candidate would immediately yield strong constraints by direct detection experiments [16, 17], and in fact reduce the signal-to-background ratio to a value too low for realistic studies. Therefore, we set the couplings in the heavy DSP cases to a value that gives similar cross sections as the corresponding light DSP scenario. This choice also simplifies comparisons between the two options.

3 Discriminative observables

The spin of the mediator can be assessed by appealing to the analytic behaviour of the scattering amplitude dictated by Regge theory [41, 42] in the limit of large invariant mass between each produced particle compared to the propagating momentum (and any mass of fields), $s_{ij} \gg |t_i|$. In this *multi-Regge kinematic* limit, which is attained within the VBF cuts, the analytic behaviour of a $2 \rightarrow n$ scattering is determined by

$$\mathcal{M}^{p_a p_b \rightarrow p_1 p_2 p_3 p_4} \rightarrow s_{12}^{\alpha_1(t_1)} s_{23}^{\alpha_2(t_2)} s_{34}^{\alpha_3(t_3)} \gamma, \tag{2}$$

p_1, \dots, p_4 are the final-state momenta ordered in rapidity, and γ depends on the couplings, the t -channel momenta t_i and ratios of $s_{ab}/(\prod s_{ij})$ only. The powers α_i determining the scaling behaviour with s_{ij} depend on the spin of the particle exchanged in the t -channel, $\alpha_i = J_i$ up to radiative corrections. In cases where the mass of the exchanged particles is negligible, the spin of the exchanged particle can therefore be inferred by studying the scaling of the cross section with the invariant mass between the electron/positron pair, see Fig. 2. Since $s_{ab} = 2p_{a\perp}p_{b\perp}(\cosh(y_a - y_b) - \cos(\phi_a - \phi_b))$, the constraint on the analytic behaviour of the scattering amplitude means that the spin of the exchanged messenger particle can be directly probed by investigating the scaling of the cross section with either the rapidity difference or the invariant mass between the electron–positron pair.

However, if the exchanged particle has a mass which is large compared to the other scales of the process, then there

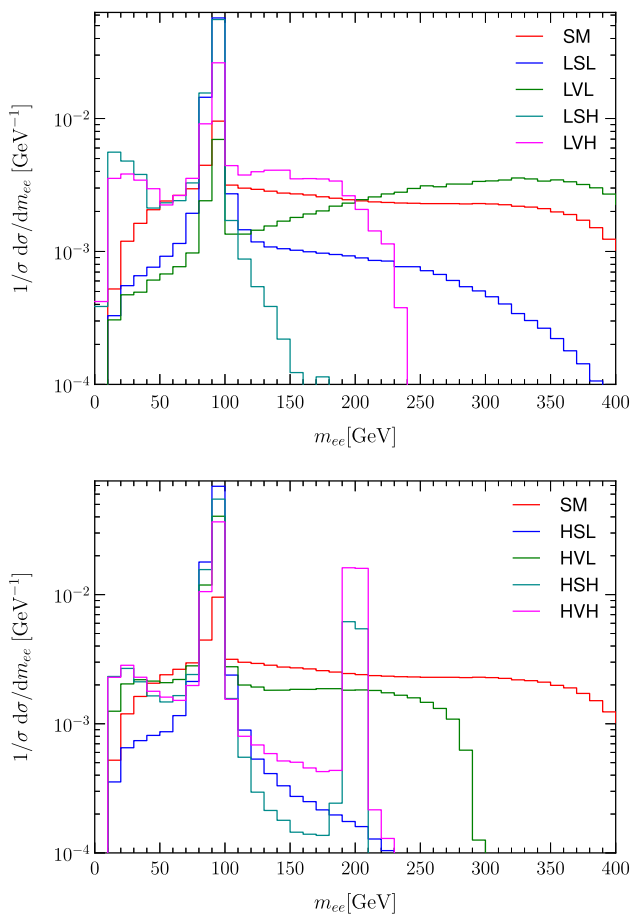


Fig. 2 $1/\sigma d\sigma/dm_{ee}$ for the Standard Model, and the models with light or heavy dark matter candidates and (top) a light mediator, (bottom) a heavy mediator. See text for more details

will be modifications to this simple picture. Other distributions would then be consulted to differentiate the spin and the mass simultaneously.

Figures 2 and 3 illustrate the different scaling of the cross section with the invariant mass of the electron-positron pair, m_{ee} , and the rapidity difference between the electron and the positron, Δy_{ee} , respectively, within our models. All shown differential cross sections are obtained from an evaluation of the full matrix elements. The predictions from the Regge analysis are observed: for a fixed setup of masses, the scalar exchange is suppressed at large m_{ee} and Δy_{ee} compared to the models with a vector mediator. While the impact of the heavy mediator mass is significant for a fixed mass of the dark matter candidate, the dominance at large Δy_{ee} (Fig. 3) of vector exchanges over scalar exchanges still holds as predicted by the Regge analysis. The same is true for $1/\sigma d\sigma/dm_{ee}$ (Fig. 2). For this distribution, two peaks in the spectrum are visible. In all cases, there is one at M_Z . This originates from diagrams which can be viewed as $Z\phi$ production, where the mediator ϕ is possibly off-shell and decays into $\chi\bar{\chi}$, and the Z subsequently decays into e^+e^- . The second peak,

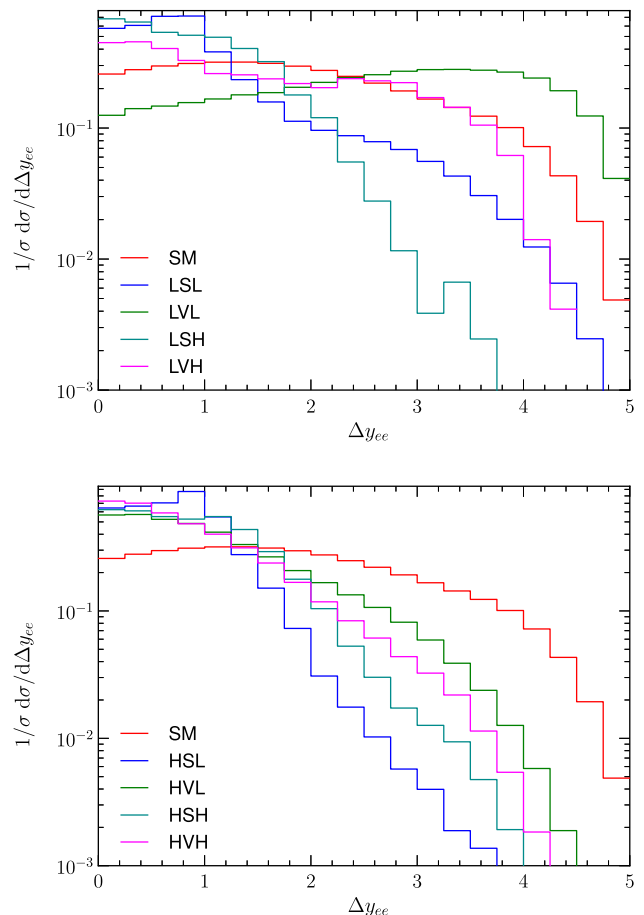


Fig. 3 $1/\sigma d\sigma/d\Delta y_{ee}$ for the Standard Model, and the models with light or heavy dark matter candidates and (top) a light mediator, (bottom) a heavy mediator. See text for more details

which is only visible for the combination of heavy mediator and heavy DSP, has its origin in diagrams where the mediator is produced on-shell together with $\chi\bar{\chi}$ and decays into e^+e^- . Such a process is in principle also possible for the other combinations, but for light DSP the heavy mediator predominantly decays into DSPs, leaving only a tiny branching fraction, and for light mediators the final-state cuts on electron and positron remove this contribution. For polarised beams, namely + polarisation of the electron beam and both possibilities for the positron beam, and vector mediators, the ratio S/B can reach 27 % (for the model LVL) at $\Delta y \geq 4$, which is where the vector like signal processes will peak.

Conversely, scalar exchange models can get S/B enhanced by studying only regions of small Δy_{ee} .

In Fig. 4 we plot the normalised differential spectrum of the invariant mass of the invisible 4-momentum in the event. This is obviously bounded from below by the sum of the masses of the two dark matter particles. If this bound is below the mass of the mediator, then the spectrum has a pronounced peak at this mass for both scalar and vector mediators. The

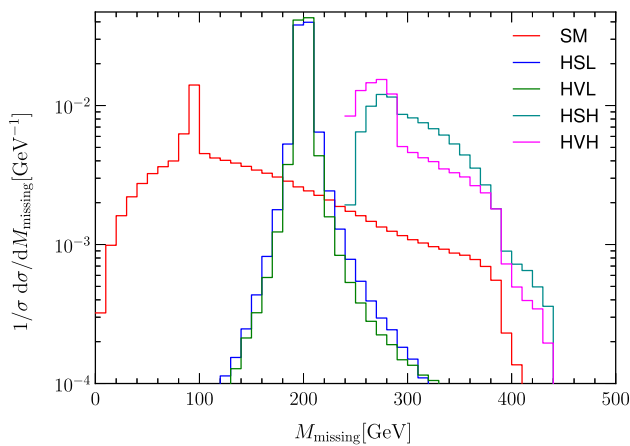
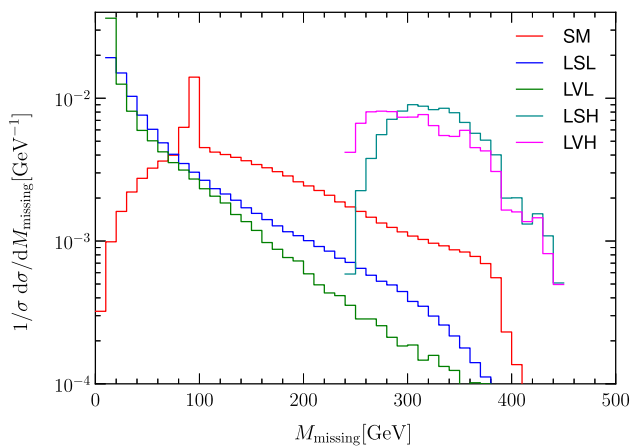


Fig. 4 $1/\sigma d\sigma/dM_{\text{missing}}$ for the Standard Model, and the models with light or heavy dark matter candidates and (top) a light mediator, (bottom) a heavy mediator. See text for more details

shape of the spectrum clearly identifies the mass-hierarchy of the mediator and DM particles: When the bound from the DM particles is above the mass of the mediator, the spectrum is very broad, as contrasted with the pronounced peak at the mediator mass.

Let us now consider shortly the case of scalar DSPs. Only those models with scalar mediator exchange give viable scenarios, where there is sufficient cross section for our signal process after the constraints from mono-photon searches have been applied. Therefore we will consider only those. We use the same setup for masses and coupling strength as in Table 2 and denote the models with an additional “S” at the beginning. Corresponding distributions are depicted in Fig. 5. The upper part shows the rapidity difference between the final-state electron and positron and corresponds to Fig. 3 for fermionic DSPs. We see that there are only small differences between the CP-even scalar and fermion DSP case. This is also expected from Regge theory, as the spin of the DSP does not enter there. In the lower part of Fig. 5 we present the invariant mass of the invisible 4-momentum, corresponding to Fig. 4 for the fermionic case. Here we do observe small differences. Probably most strik-

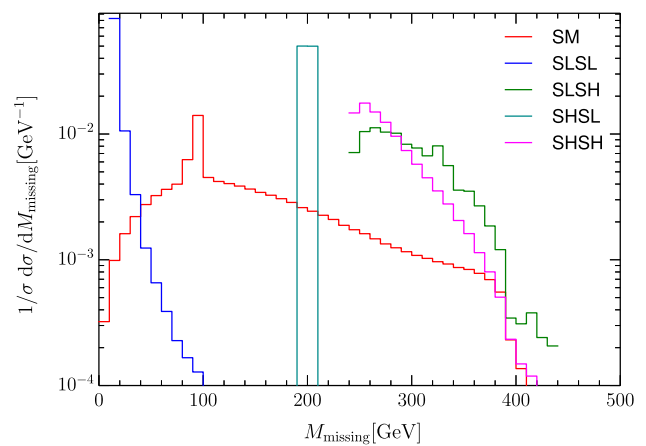
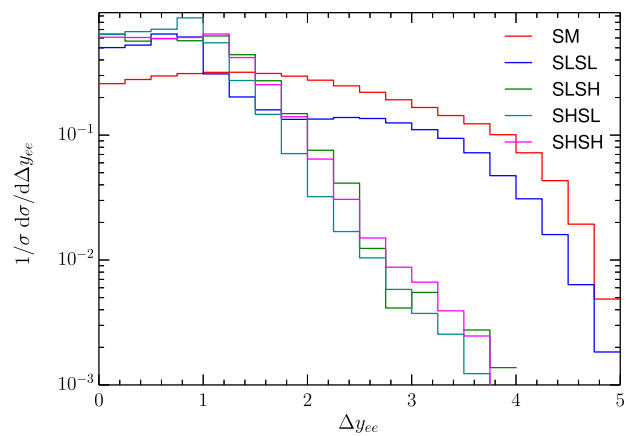


Fig. 5 $1/\sigma d\sigma/d\Delta y_{ee}$ (top) and $1/\sigma d\sigma/dM_{\text{missing}}$ for scalar CP-even DSPs, scalar mediator particle and different mass scenarios of the two particles. See text for more details

Table 3 Cross sections in femtobarn for the different models imposing the constraints as outlined in the text. The three columns refer to the three different beam polarisations: averaged, ++ and +-. The first index refers to the electron beam which we assume to be able to polarise 80 % (always +). The second index represents the positron beam which we assume to have a polarisation degree of 30 %. The cross sections vary between (0.7–13.0, 1.3–26.1, 2.4–46.8 %) of the Standard Model background for three polarisations (all, ++, +-), respectively

Model	σ_{unpol}	σ_{++}	σ_{+-}
SM	115.8	49.1	36.4
LSL	1.60	1.79	1.40
LVL	15.07	12.80	17.02
LSH	1.45	1.80	1.10
LVH	9.99	7.64	12.33
HSL	1.17	1.43	0.92
HVL	0.85	0.71	0.89
HSH	1.18	1.45	0.90
HVH	0.85	0.64	0.98

ing is the SHSL model, which is, however, simply an effect of the different width of the mediator particle, which is predominantly produced on-shell. With large enough statis-

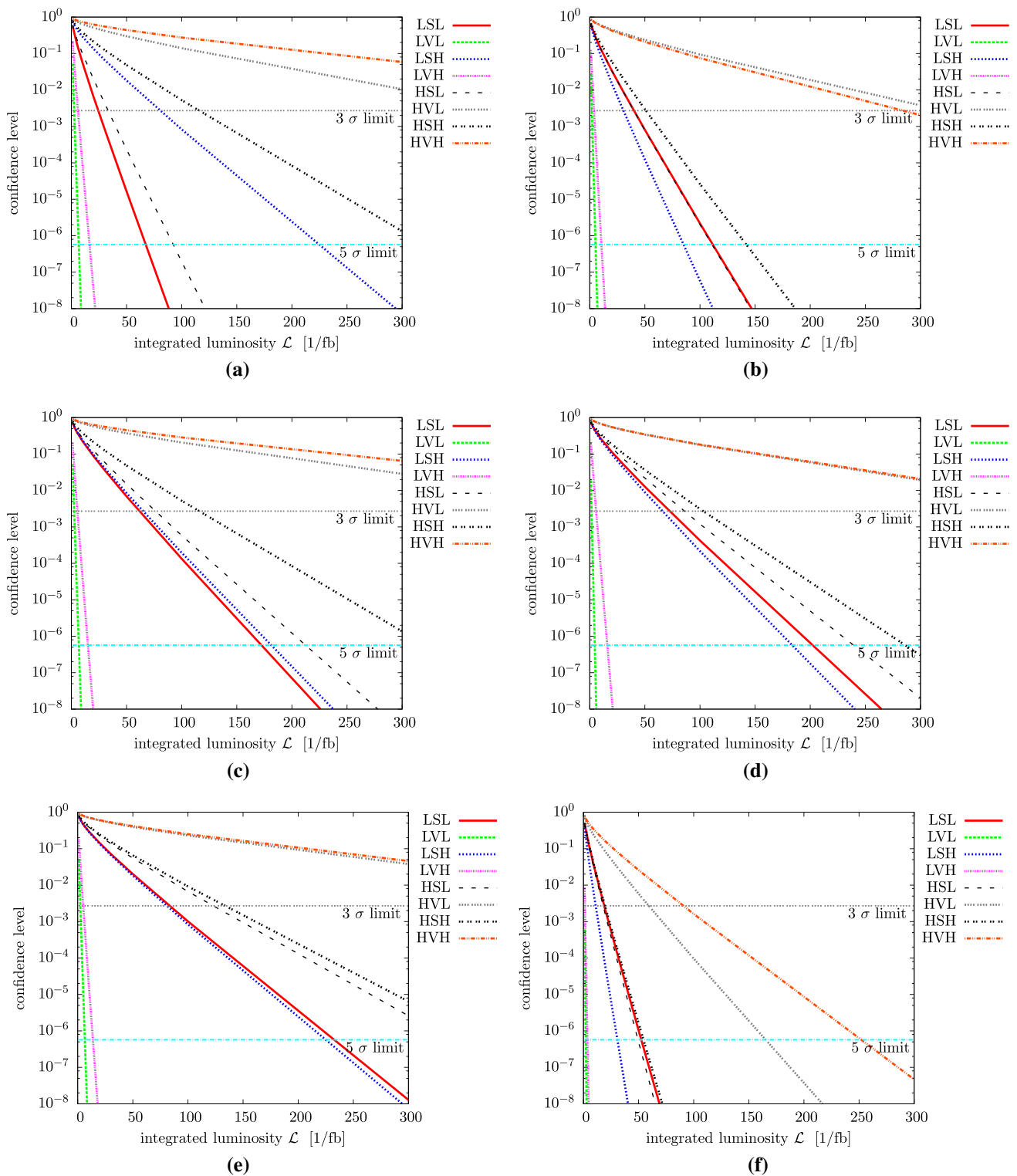


Fig. 6 Assuming realisation of the Standard Model only, these plots show the confidence level to which the respective Dark Sector model can be disfavoured using just one observable. The curves take into account not only the shapes but also the normalisation of the model’s cross sec-

tion. **a** Missing transverse energy, **b** invariant mass of e^+e^- system, **c** $\Delta\phi_{e^+e^-}$, **d** $\Delta y_{e^+e^-}$, **e** p_T of hardest lepton, **f** invariant mass of DSP system, M_{missing}

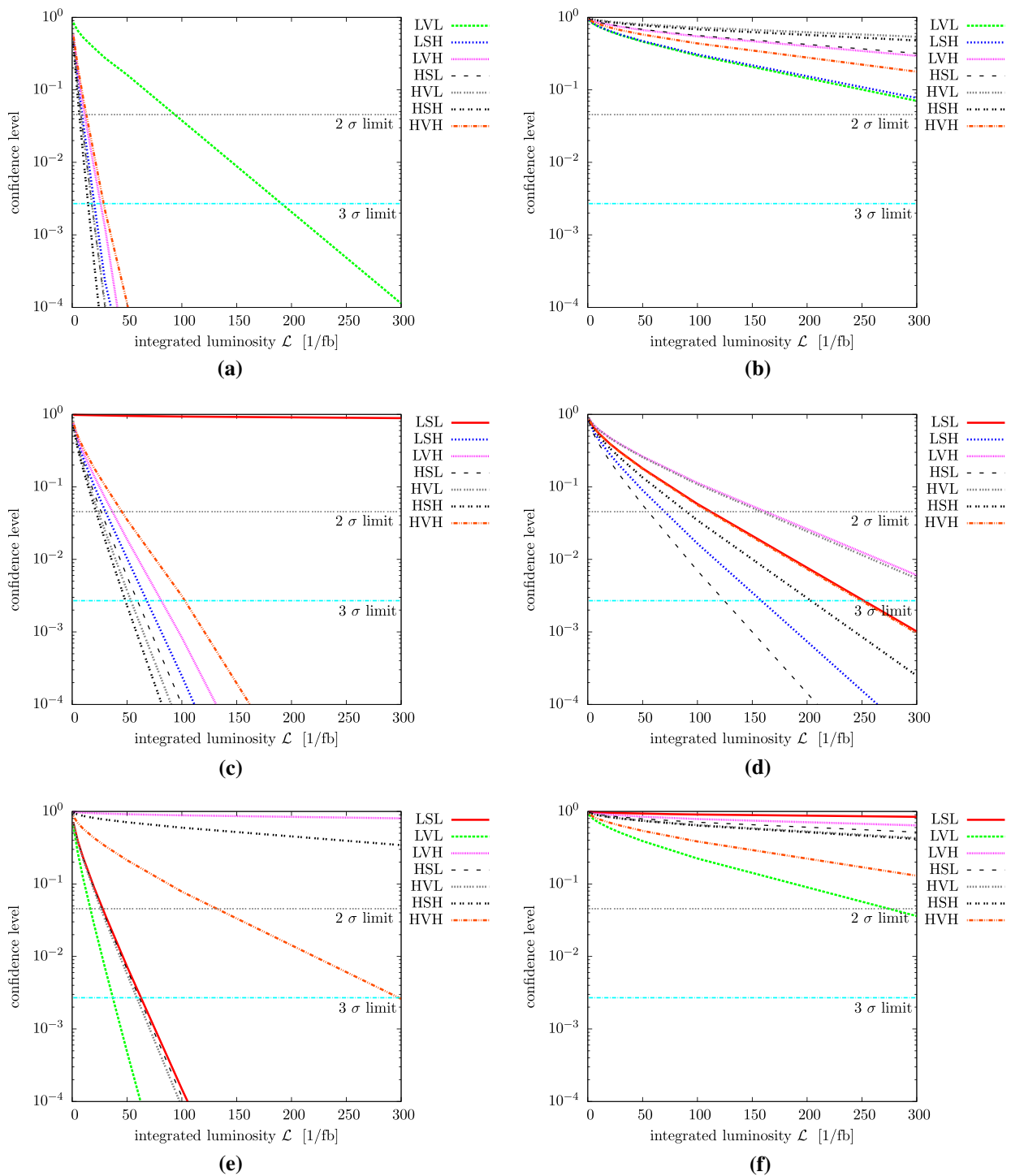


Fig. 7 The curves illustrate the level to which the M_{missing} and $m_{e^+e^-}$ can discriminate between the different models, assuming the realisation of LSL (a–b), LVL (c–d), LSH (e–f), LVH (g–h), HSL (i–j), HVL (k–l), HSH (m–n) and HVH (o–p). All cross sections are assumed to be 2.5 % of the Standard Model background cross section. **a** M_{missing} for LSL, **b** invariant mass of e^+e^- system for LSL, **c** M_{missing} for LVL, **d**

invariant mass of e^+e^- system for LSH, **e** M_{missing} for LVH, **f** invariant mass of e^+e^- system for LSH, **g** M_{missing} for LVH, **h** invariant mass of e^+e^- system for LVH, **i** M_{missing} for HSL, **j** invariant mass of e^+e^- system for HSL, **k** M_{missing} for HVL, **l** invariant mass of e^+e^- system for HVL, **m** M_{missing} for HSH, **n** invariant mass of e^+e^- system for HSH, **o** M_{missing} for HVH and **p** invariant mass of e^+e^- system for HVH

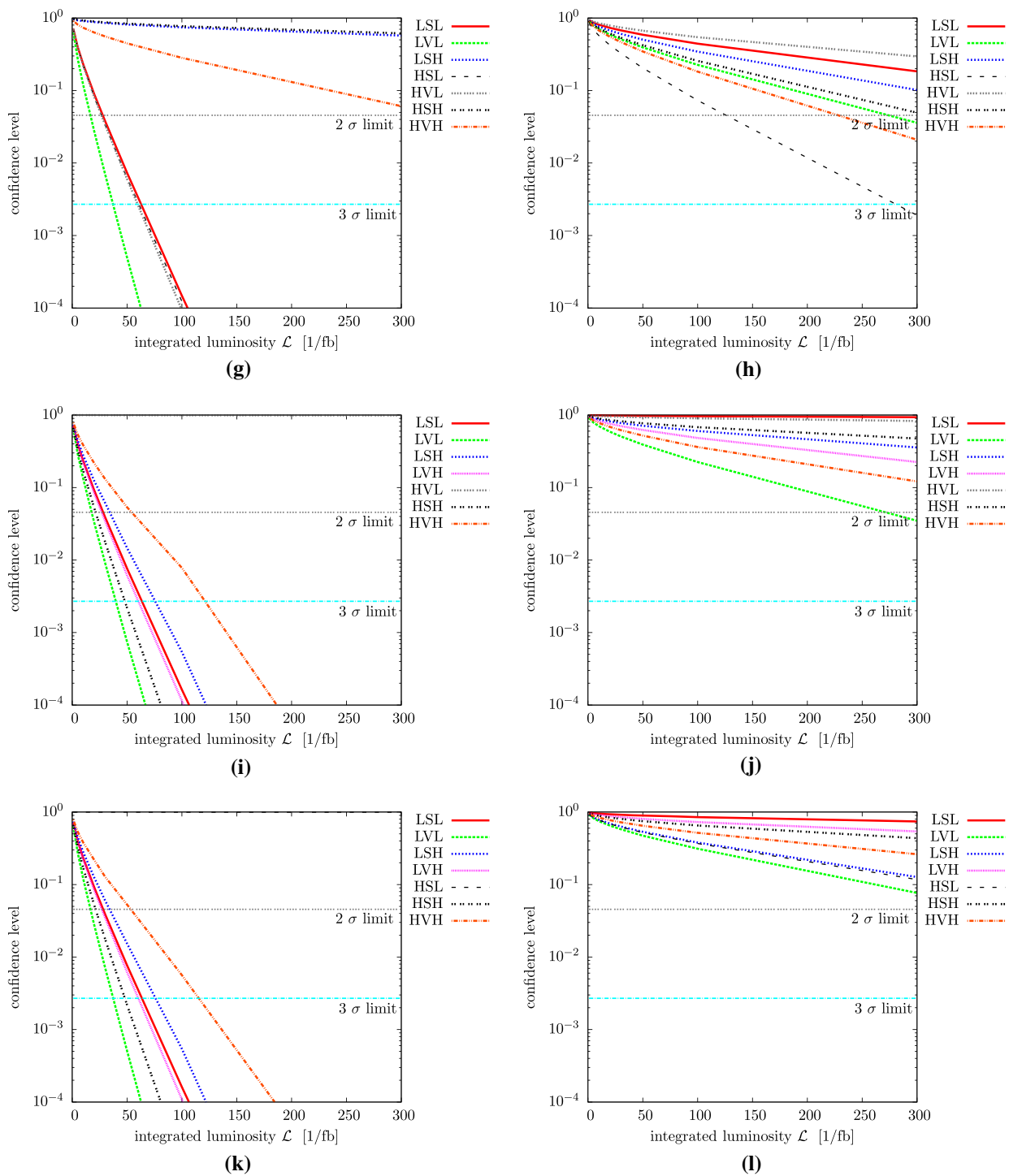


Fig. 7 continued

tics, these differences could eventually be exploited for a distinction of scalar and fermionic dark matter. In the following, we will, however, concentrate on the much larger effects induced by the spin of the mediator and the different masses.

In case we studied scalar CP-odd DSPs, $\Delta\phi_{e^-e^+}$ can be helpful for their discrimination. For the eight models with

fermionic DSPs we study here, $\Delta\phi_{e^-e^+}$ is of minor importance.

In conclusion, the distribution of the invariant mass of the invisible momentum, M_{missing} can uniquely determine the mass scale and hierarchies of the mediator and dark matter particle, but does not discriminate between scalar and vector mediators. However, once the mass scales are determined,

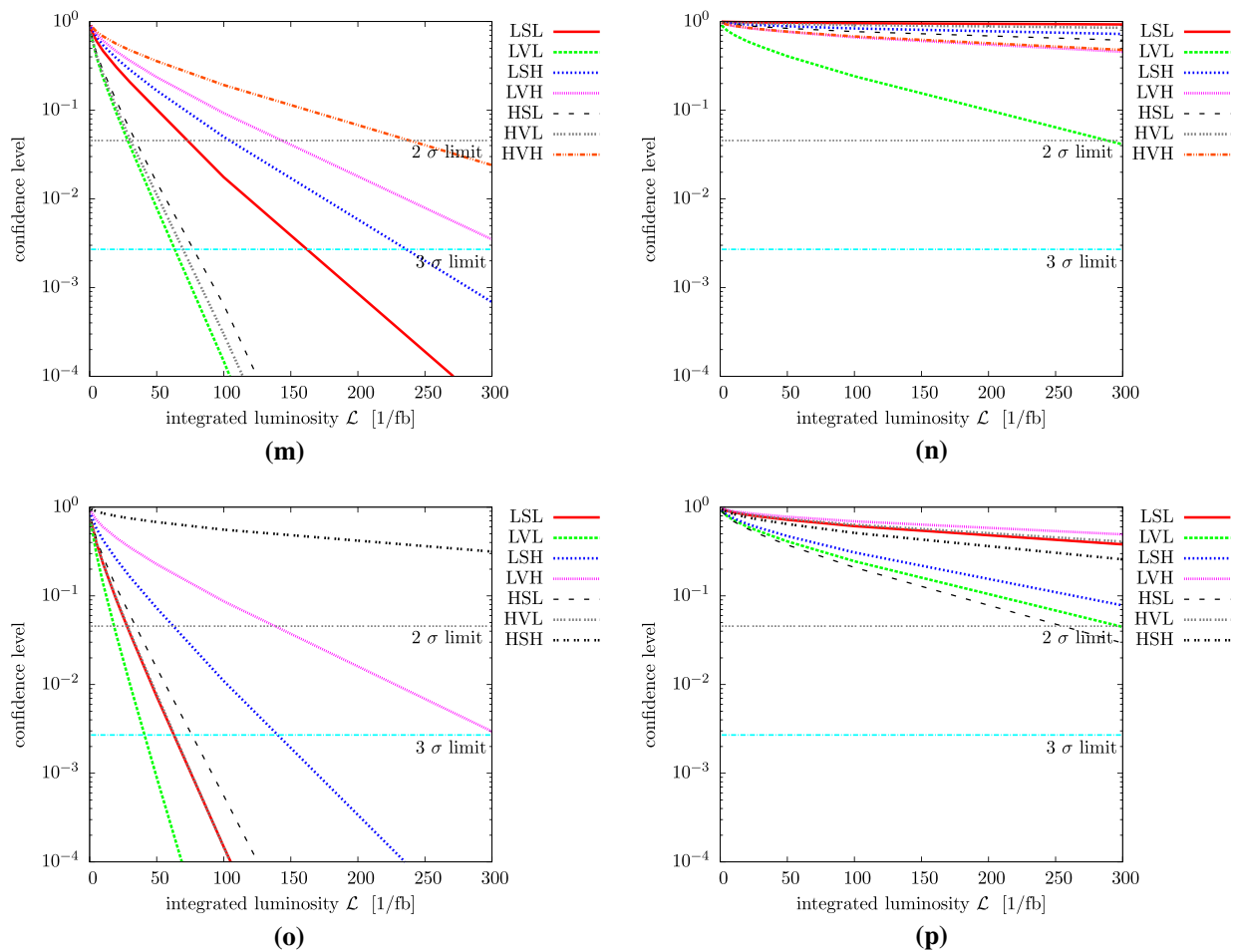


Fig. 7 continued

the spin of the mediator can be determined from the shape of the cross section with respect to Δy_{ee} or equivalently m_{ee} , due to the spin-dependence dictated by the Regge analysis. Other distributions on e.g. the transverse momentum of the hardest lepton can then be used to check for consistency.

4 Discriminating models

As discussed in Sect. 3, we expect the observables $m_{e^+e^-}$ and the invariant mass of the DSPs, precisely measured as recoil system of e^+e^- , to be the strongest discriminators for the benchmark models. At the ILC the lepton’s energy is precisely determined and the beams can be partly polarised. We assume conservatively that the degree of polarisation is 80 % for the electrons and 30 % for the positrons [43]. In Table 3 we show the cross section for three different beam polarisations: unpolarised, ++ and +-. The first (second) index refers to the electron (positron) beam. Only fairly inclusive cuts have been placed on the final-state particles, namely $p_{T,e^+,e^-} > 20 \text{ GeV}$, $|\eta_{e^+,e^-}| < 2.5$, $R_{e^+e^-} > 0.4$ and

$E_{T,\text{miss}} > 50 \text{ GeV}$. We find that the ratio between signal and background cross section can be improved for all models by using polarised beams.

Note, the signal models’ cross sections respond differently to a change in the polarisation of the beams. Hence the inclusive production cross section can be used to discriminate between the models as well, i.e. for scalar mediators $\sigma_{++} > \sigma_{\text{unpol}}$ while for vector mediators $\sigma_{+-} > \sigma_{\text{unpol}}$. However, in this work we will focus on the observables identified in Sect. 3 only and because of the recent interest in vector mediators [37–40] we will choose the +- beam polarisation in the following.

We perform a binned log-likelihood hypothesis test [44–47] using the CL_S method [48, 49] to evaluate how well the eight benchmark models can be discriminated from each other and from the Standard Model. For the graphs in Fig. 6 we assume only the Standard Model is realised in nature. Hence, the Standard Model is used as a background hypothesis in the CL_S analysis. Due to the large allowed cross section of the LVL and LVH models they can be excluded for the given coupling strength with less than 10 fb^{-1} . However,

with an integrated luminosity of roughly 300 fb^{-1} all models can be disfavoured at the 5σ confidence level.

For the results shown in Fig. 7 we assume, respectively, that one of the models is realised in nature, as indicated by the caption of each sub-figure. Thus, the distributions used for the CL_S method consist of the sum of the Standard Model and the respective benchmark model distribution, i.e. we take the statistical uncertainty of the Standard Model distributions into account for the hypothesis test, while we neglect interference effects between the Standard Model and the new physics scenarios. The coupling strength in each model is chosen such that it is respecting present bounds. However, as discussed in Sect. 2, bounds from direct and indirect detection experiments can be avoided in case the DSPs are not stable on cosmological time scales. Only bounds from direct searches at LEP pose a stringent constraint. To evaluate how well the different quantum numbers of the benchmark models can be discriminated we assume all benchmark models have a cross section of 2.5 % of the Standard Model cross section. All CL_S results are based on the distributions of Figs. 2, 3, 4 and 5.

We have studied the impact of all the observables shown in Fig. 6, namely missing transverse energy, $m_{e^+e^-}$, $\Delta\phi_{e^+e^-}$, $\Delta y_{e^+e^-}$, p_T of the hardest lepton and M_{missing} . We find that $m_{e^+e^-}$ and M_{missing} are sufficient to discriminate the quantum numbers of our candidate models confidently. M_{missing} gives a handle on the mass scales, while $m_{e^+e^-}$ discriminates the spin of the mediators. This is clearly demonstrated by comparing Fig. 7c and 7d, where LVL and LSL are strongly discriminated by including $m_{e^+e^-}$ whereas M_{missing} has almost no discriminating power. The situation is reversed for the discrimination of LSL and LSH, as shown in Fig. 7e and 7f. Here both, LSL and LSH have a pronounced peak in $m_{e^+e^-}$ at the Z boson mass (thus $m_{e^+e^-}$ is not discriminating the two models), but the large difference of the DSP mass is reflected in $M_{\text{missing}} \geq 2M_{\text{DSP}}$. However, if one wants to discriminate quantum numbers beyond mass and spin (e.g. CP structure) other observables should be included, e.g. $\Delta\phi_{e^+e^-}$. A combination of the variables discussed will improve the statistical significance in discriminating the models' quantum numbers.

In general and in particular for a leptophilic scenario, studying a dark sector using t -channel mediated forces is a challenging task at the LHC. This study has demonstrated that even with conservative assumptions on the level of polarisation, the ILC can conclusively explore the quantum numbers of a dark sector by using a combination of M_{missing} and $m_{e^+e^-}$.

Acknowledgments MR acknowledges partial support by the Deutsche Forschungsgemeinschaft via the Sonderforschungsbereich/Transregio SFB/TR-9 "Computational Particle Physics" and the Initiative and Networking Fund of the Helmholtz Association, contract HA-101 ("Physics at the Terascale").

Open Access This article is distributed under the terms of the Creative Commons Attribution License which permits any use, distribution, and reproduction in any medium, provided the original author(s) and the source are credited.

Funded by SCOAP³ / License Version CC BY 4.0.

References

- G. Bertone, D. Hooper, J. Silk, Phys. Rep. **405**, 279 (2005). ([hep-ph/0404175](#))
- E. Komatsu et al., WMAP collaboration. Astrophys. J. Suppl. **192**, 18 (2011) ([arXiv:1001.4538](#) [astro-ph.CO])
- L. Bergstrom, Ann. Phys. **524**, 479 (2012). ([arXiv:1205.4882](#) [astro-ph.HE])
- P.A.R. Ade et al., Planck collaboration ([arXiv:1303.5062](#) [astro-ph.CO])
- P.A.R. Ade et al., Planck collaboration ([arXiv:1303.5076](#) [astro-ph.CO])
- P. Picozza, A.M. Galper, G. Castellini, O. Adriani, F. Altamura, M. Ambriola, G.C. Barbarino, A. Basili et al., Astropart. Phys. **27**, 296 (2007)
- O. Adriani et al., PAMELA collaboration. Nature **458**, 607 (2009)
- M. Ackermann et al., Fermi LAT collaboration. Phys. Rev. Lett. **108**, 011103 (2012) ([arXiv:1109.0521](#) [astro-ph.HE])
- M. Aguilar et al., AMS collaboration. Phys. Rev. Lett. **110**(14), 141102 (2013) (main results at <http://www.ams02.org/>)
- P.J. Fox, E. Poppitz, Phys. Rev. D **79**, 083528 (2009). ([arXiv:0811.0399](#) [hep-ph])
- M. Cirelli, M. Kadastik, M. Raidal, A. Strumia, Nucl. Phys. B **813**, 1 (2009) (addendum-ibid. B **873**, 530, 2013) ([arXiv:0809.2409](#) [hep-ph])
- C.-R. Chen, F. Takahashi, JCAP **0902**, 004 (2009). ([arXiv:0810.4110](#) [hep-ph])
- M.J. Strassler, K.M. Zurek, Phys. Lett. B **651**, 374 (2007). ([hep-ph/0604261](#))
- D.E. Kaplan, M.A. Luty, K.M. Zurek, Phys. Rev. D **79**, 115016 (2009). ([arXiv:0901.4117](#) [hep-ph])
- T. Cohen, K.M. Zurek, Phys. Rev. Lett. **104**, 101301 (2010). ([arXiv:0909.2035](#) [hep-ph])
- C. Savage, G. Gelmini, P. Gondolo, K. Freese, Phys. Rev. D **83**, 055002 (2011)
- J.M. Cline, Z. Liu, W. Xue, Phys. Rev. D **87**, 015001 (2013)
- A. Birkedal, K. Matchev, M. Perelstein, Phys. Rev. **D70**, 077701 (2004). ([hep-ph/0403004](#))
- J.L. Feng, S. Su, F. Takayama, Phys. Rev. Lett. **96**, 151802 (2006). ([hep-ph/0503117](#))
- M. Beltran, D. Hooper, E.W. Kolb, Z.C. Krusberg, Phys. Rev. D **80**, 043509 (2009). ([arXiv:0808.3384](#) [hep-ph])
- Q.-H. Cao, C.-R. Chen, C.S. Li, H. Zhang, JHEP **1108**, 018 (2011). ([arXiv:0912.4511](#) [hep-ph])
- M. Beltran, D. Hooper, E.W. Kolb, Z.A.C. Krusberg, T.M.P. Tait, JHEP **1009**, 037 (2010). ([arXiv:1002.4137](#) [hep-ph])
- J. Goodman, M. Ibe, A. Rajaraman, W. Shepherd, T.M.P. Tait, H.-B. Yu, Phys. Lett. **B695**, 185–188 (2011). ([arXiv:1005.1286](#) [hep-ph])
- Y. Bai, P.J. Fox, R. Harnik, JHEP **1012**, 048 (2010). ([arXiv:1005.3797](#) [hep-ph])
- P.J. Fox, R. Harnik, J. Kopp, Y. Tsai, Phys. Rev. D **84**, 014028 (2011). ([arXiv:1103.0240](#) [hep-ph])
- A. Rajaraman, W. Shepherd, T.M.P. Tait, A.M. Wijangco, Phys. Rev. D **84**, 095013 (2011). ([arXiv:1108.1196](#) [hep-ph])
- P.J. Fox, R. Harnik, J. Kopp, Y. Tsai, Phys. Rev. D **85**, 056011 (2012)
- H. Dreiner, M. Huck, M. Kramer, D. Schmeier, J. Tattersall, Phys. Rev. D **87**, 075015 (2013). ([arXiv:1211.2254](#) [hep-ph])

29. ILC Technical Design Report, ILC collaboration. <http://www.linearcollider.org/ILC/Publications/Technical-Design-Report>. (arXiv:1306.6352 [hep-ph])
30. G. Aarons et al., ILC collaboration (arXiv:0709.1893 [hep-ph])
31. T. Plehn, D.L. Rainwater, D. Zeppenfeld, Phys. Rev. Lett. **88**, 051801 (2002). (hep-ph/0105325)
32. G. Klamke, D. Zeppenfeld, JHEP **0704**, 052 (2007). (hep-ph/0703202 [hep-ph])
33. J.R. Andersen, K. Arnold, D. Zeppenfeld, JHEP **1006**, 091 (2010). (arXiv:1001.3822 [hep-ph])
34. O.J.P. Eboli, D. Zeppenfeld, Phys. Lett. **B495**, 147–154 (2000). (hep-ph/0009158)
35. H. An, L.-T. Wang, H. Zhang (arXiv:1308.0592 [hep-ph])
36. P. Meade, M. Reece (hep-ph/0703031)
37. B. Holdom, Phys. Lett. B **166**, 196 (1986)
38. R. Foot, X.-G. He, Phys. Lett. B **267**, 509 (1991)
39. S.A. Abel, M.D. Goodsell, J. Jaeckel, V.V. Khoze, A. Ringwald, JHEP **0807**, 124 (2008)
40. N. Arkani-Hamed, N. Weiner, JHEP **0812**, 104 (2008)
41. T. Regge, Nuovo Cim. **14**, 951 (1959)
42. R.C. Brower, C.E. DeTar, J.H. Weis, Phys. Rep. **14**, 257 (1974)
43. M.E. Peskin (ed.) et al., Physics at the International Linear Collider, ILC Detailed Baseline Design Report (2013)
44. T. Junk, Nucl. Instrum. Method A **434**, 435 (1999)
45. T. Junk, CDF Note 8128 (cdf/doc/statistics/public/8128)
46. T. Junk, CDF Note 7904 (cdf/doc/statistics/public/7904)
47. H. Hu, J. Nielsen, in 1st Workshop on Confidence Limits, CERN 2000–005 (2000)
48. A.L. Read, CERN-OPEN-2000-205
49. A.L. Read, J. Phys. G **G28**, 2693–2704 (2002)